NUCLEAR SCIENCE AND ENGINEERING 109 (1991) PG. 267-277

A Neutron Source Imaging Detector for Nuclear Arms Treaty Verification

W. C. Sailor, R. C. Byrd, A. Gavron, and R. Hammock
Los Alamos National Laboratory, Los Alamos, New Mexico 87545

and

Y. Yariv
Soreq Nuclear Research Center, Yavne 70600, Israel

Received October 25, 1990
Accepted February 13, 1991

Abstract – *A detector design that is capable of finding the image of neutron sources within a nuclear missile is discussed. The method involves the double scatter of a neutron in an array of organic scintillator elements and the partial reconstruction of the incident neutron direction vector from the information the array provides. The Monte Carlo simulation results for a basic design and several modifications are presented. The results of an experimental demonstration of the technique using a crude prototype detector are given. Problems expected in a real application are discussed.*

I. INTRODUCTION

In future nuclear arms reduction treaties, there may be the need to provide a method of verifying or counting the number of nuclear warheads contained within a given missile. Our motivation for working on this type of detector stems from our support of a treaty verification program at Los Alamos National Laboratory where we are investigating the detection of the neutrons emitted in spontaneous fission and (α, n) reactions.

The method involves the double scatter of neutrons from cells of organic scintillator material and is similar to a method used in the detection of atmospheric or solar neutrons.[1,2] The two hit positions, the pulse height associated with the proton recoil in the first cell, and the time of flight (TOF) of the neutron between the two scatters are used to partially reconstruct the incident neutron momentum vector. An incident neutron energy is also obtained. An image of a nearby neutron source or sources is obtained after several thousand events.

Our approach is primarily through the use of a Monte Carlo code to investigate the performance of conceptual detector designs. Because the true application is quite complicated by the warhead and missile designs and by political considerations, we do not develop an optimum design but rather study the simulated imaging performance of a few reasonable designs. We also demonstrate the feasibility of the method by experimental investigations using a crude prototype detector with a laboratory ^{252}Cf (spontaneous fission) source. Several problems unforeseen by the Monte Carlo studies are encountered in the experiments.

In this paper, we discuss a possible detector configuration and develop the basic physics involved in the imaging scheme. The resolution effects expected in a real detector are discussed. The results of several detector simulations that include model resolution effects are given. The result of an experimental demonstration using a prototype detector and a spontaneous fission neutron source is shown and compared to a Monte Carlo result. Finally, some of the issues in constructing a real detector system are discussed.

II. CONCEPTUAL DETECTOR CONFIGURATION

Figure 1 shows a schematic view of a detector configuration. There are two planes of plastic scintillator, each a few centimetres thick, subdivided into individual elements 1 to 10 cm on a side. Neutrons scatter sequentially from the hydrogen nuclei in the first plane and then the second. Each element has a photomultiplier (PM) tube and associated electronics needed to determine the pulse height and timing of neutron events in the cells. The neutrons pass through the PM tubes when traveling from the first plane to the second, with a small probability of scattering in the tube material. The trigger is formed from a coincidence between the two planes (i. e., a logical "AND" between the "OR" of all cells in the first plane and the "OR" of all cells in the second plane). A computer is used to evaluate the data from each trigger on an event-by-event basis.

Figure 2 illustrates the geometry assumed for the partial reconstruction of the incident neutron direction. A source neutron is incident on the front face of the detector at an angle γ relative to the normal of the detector plane, scatters from a proton in the first plane at a reaction angle $\alpha + \gamma$ (the proton angle is β), and is detected in a second plane. The angle α (of the scattered neutron in the detector coordinate system) is determined from the known hit positions. For each event, the scattered neutron's energy E_n is known from its TOF between planes. The pulse amplitude for the scatter in the front plane is converted to a proton energy E_p by use of a light output curve for protons in the scintillator material. The proton scattering angle is found from the kinematical relation $\beta = \arctan[(E_n/E_p)^{1/2}]$. The angle γ is then found from the geometric relation $\alpha + \beta + \gamma = 90$ deg.

From the foregoing information, the incident neutron hit position and incident angle are known (additionally the incident energy is known from $E_i = E_n + E_p$). This information is not complete enough to uniquely determine the incident neutron direction. However, the locus of all possible incident directions for that neutron is a *cone* with its apex at the point of interaction in the first plane, its axis along the scattered neutron flight path, and its opening angle equal to $\alpha + \gamma$. The locus of all possible source positions is also this same cone in space.

After many events occur, the overlap of the cones begins to form an image. If there is an estimate of one of the coordinates of the source (for instance, if one knows the linear distance from the detector to the source), then the imaging problem is reduced to two dimensions. Thus, the cones are projected into the plane defined by the known coordinate, and a conic section, such as an ellipse or hyperbola, results for each event. After many events, the conic sections tend to overlap at the location of the source in that plane.

Figure 3 shows the results of a Monte Carlo simulation of how an idealized detector with perfect position, timing, and pulse-height resolution would find the location of a point source placed at the origin of a plane parallel to the detector planes. There are 15 detected neutrons from a point source at the origin of the plane, which is parallel to the detector planes. In this geometry, the intersections of the cones with this plane form ellipses that all cross through the origin. If the source were instead at some other location in the plane, the ellipses would cross at that point.

A scheme to locate neutron sources in three-dimensional space is a generalization of this method. A method to view the overlapping cones from different projections is needed, and different shading or

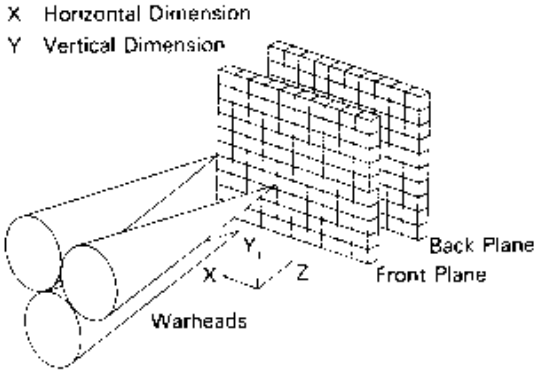

Fig. 1. Schematic view of an imaging detector.

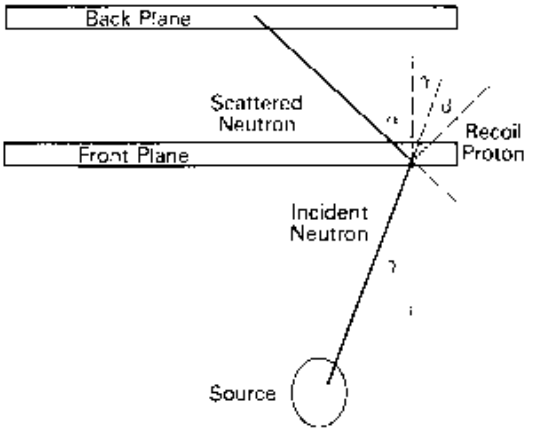

Fig. 2. A simplified, two-dimensional version of the geometry assumed for the neutron's double scatter in the detector. The scattered proton energy in the front plane is found from the pulse amplitude, and the scattered neutron energy is found from the neutron TOF between planes.

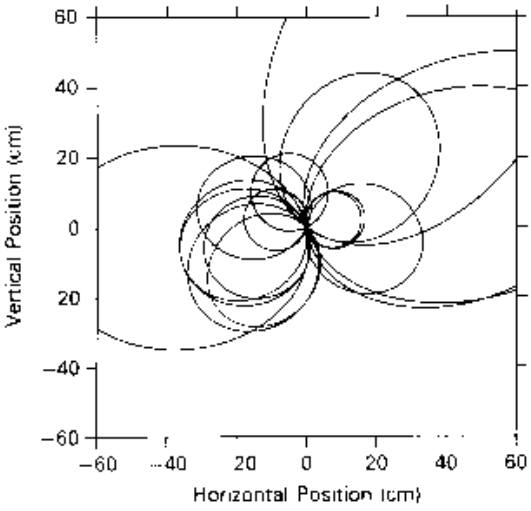

Fig. 3 Monte Carlo simulation of how an idealized detector with perfect position, timing, and pulse-height resolution would be used to find the location of a point source placed at the origin of a plane parallel to the detector planes.

colors could represent the density of the cones per unit volume.

III. FACTORS INFLUENCING IMAGE RESOLUTION

A sharp, pointlike image as described in Sec. II cannot be expected from a real detector. Instead, the imaging capability is limited by instrumental resolution effects that are the result of the finite cell size, the presence of carbon and other materials within and nearby the scintillator material, and the photon yield of organic scintillators. In addition, if the neutron-producing reaction in the source generates multiple neutrons or produces other particles that interact in the detector, the image quality can also be affected by coincidences between these particles.

The cell size affects not only the uncertainty in the location of the cone apex but also the flight distance for the neutron between scatters. For mega-electron-volt-range neutrons, the mean-free-path in NE-102 scintillator material is ~5 cm, and therefore the optimum cell thickness that maximizes detection efficiency yet suppresses multiple scattering is on the order of a few centimetres. The flight distance uncertainty is roughly equal to half the cell thickness, so if the gap between planes is at least four times the cell thickness, this "cell size" contribution to the scattered neutron energy resolution is <20%.

The scattering probabilities in organic scintillator for mega-electron-volt-range neutrons are about equal for protons compared with carbon. The carbon scattering reaction changes the direction of the neutron and decreases its energy slightly while producing virtually no light. Because of the small neutron/carbon mass ratio, the neutron tends to scatter through a large angle. If such a scatter occurs, the reconstructed incident neutron vector is greatly changed.

The same applies for scatters on PM tubes or structural framework. The neutrons must pass through the tubes on the back side of the front plane to reach the second plane, and any scatter tends to destroy the information in the event. However, typical tube masses (without magnetic shielding) are <15 g. Assuming the tubes are half SiO_2 and half iron, the scattering probability is estimated to be <3% for the configurations discussed in this paper, which represents only a small loss in efficiency.

The pulse-height and the timing resolutions are both governed primarily by the number of photoelectrons generated in the photocathodes of the PM tubes, which is a small number in any organic scintillator detecting few mega-electron-volt proton recoils. Cells should therefore be designed for optimum light collection properties. Through the use of metallic wrappings or coatings, it may be possible to collect 30% or more of the light generated in an optimal cell. Other factors influencing the pulse-height resolution are the variation in the light collection efficiency throughout the volume of the cell, the PM tube gain dispersion, and the electronic noise.[3]

Coincidences between two particles emitted in the same reaction are possible and, under the condition of high absolute singles detection efficiency, are numerically comparable with the true double scatters. Because the cones calculated for these events are calculated incorrectly, such false coincidences will contribute to a broadening of the true image. In the case of ^{252}Cf spontaneous fission, an average of 3.8 neutrons[4] and ~9.7 gamma rays is emitted per fission.[5] For ^{240}Pu these numbers are ~2.3 and 7 per fission, respectively.[6] Neutrons emitted in (α,n) reactions can be accompanied by one or two gamma rays. A gamma ray interacting in the front plane in combination with a neutron interacting in the second plane sometimes passes as a neutron double scatter. An additional coincidence mode, of concern at least with a ^{252}Cf source, is a single scatter in the front plane for one neutron and single scatter in the second plane for another.

Other gamma-ray coincidences, such as a gamma-ray double scatter or a scatter in each plane by different gamma rays, can be eliminated based on the apparent TOF between planes, provided the detector has reasonably good timing resolution and the plane spacing is kept above a reasonable minimum. This elimination is possible because >90% of the gamma rays emitted in the fission process are produced in the

first nanosecond after the fission[6] and because mega-electron-volt-range neutron flight times are typically at least ten times that of photons over the same flight path.

IV. SIMULATION OF DETECTOR CONFIGURATIONS

To explore the effects of various detector imperfections and quantify detector performance regarding cell dimensions, gaps, neutron energies, and source-detector geometries, a Monte Carlo code[7] is employed. The code, which is a descendant of a code[8] used to simulate single-cell neutron detectors in low- and medium-energy physics for many years, is specially adapted to the multicell, multiplane configuration. Included in the code are neutron interactions on protons and carbon and pulse height and timing jitter effects due to photoelectron statistics. The proton light output curve used in the simulation is taken from the literature.[9] For more details about the code, see Refs. 7 and 8.

A detector similar to that shown in Fig. 1 is simulated using mostly realistic assumptions about the detector properties. Here the elements are made of NE-102 commercial scintillator, 4 cm thick, 4 cm high, and 5 cm long, which are arranged in a 10×10 grid in each plane. The planes are separated by a 12-cm gap, and the source is 40 cm from the front of the first plane.

The energy spectrum of the source is taken from Ref. 10.[a] This distribution could also represent that of the spontaneous fission spectrum of any of the isotopes of plutonium or of the thermal neutron induced fission spectrum of ^{235}U or ^{239}Pu. The distribution has a mean energy of ~2.36 MeV and a significant intensity up to ~10 MeV.

The pulse-height resolution can be estimated as follows.[3] A 1-MeV proton stopping in NE-102 produces only ~100-keV-electron equivalent (or keV_{ee}) of light output.[11] Assuming an optimistic value of 9800 photons/MeV_{ee} produced,[12,b] 15% light collection efficiency, and a 25% quantum efficiency, the result is only 37 photoelectrons. Poisson statistics would indicate a standard deviation of 16% in pulse height. The effects of an expected 45% dispersion in the PM tube gain and 10% geometrical variation in the light collection efficiency worsens the resolution somewhat beyond this, giving a pulse-height resolution of ~20%.

The timing resolution is given roughly as one-half the product of the scintillator decay time and the fractional pulse-height resolution.[13,c] The scintillator material NE-102 has a decay time of 2.4 ns and therefore will have a timing resolution of about $\sigma = 0.25$ ns for the aforementioned 1-MeV proton. This value translates into about 0.35 ns in TOF resolution when both tubes are counted. However, the flight time for a 1-MeV neutron over a 20-cm gap is 15 ns; therefore, this timing jitter is an insignificant contribution to the scattered neutron energy resolution compared with the flight path uncertainty from the finite cell size.

In the simulation, assumptions about pulse height and timing jitter were made that were consistent with the foregoing two paragraphs. A value of 367 photoelectron/MeV_{ee} of light generated in the cell was assumed. Gain dispersion in the PM tube was taken as $\sigma_{PM} = 45\%$. The timing resolution on a given cell was taken as $\sigma = 0.08/L^{1/2}$ ns where L is the light output in MeV_{ee}.

There are two tests (or cuts) required by the analysis software. To reconstruct the energy of the scattered neutron in an unambiguous fashion, it is required that one cell only per plane can have a hit. If there is a greater number than this, the event is discarded on the basis of multiplicity. Between 5 and 10% of events were eliminated by the multiplicity cut. Also, discriminator thresholds were simulated by requiring a minimum of 130 keV_{ee} pulse height in each cell.

The simulation of several ellipses that would result from this detector when used with a point source located at a position (+15 cm, +15 cm) in the plane is shown in Fig. 4. The finite cell size, carbon scattering, and pulse height and timing resolution contribute to irreducible random errors in determining the ellipses, so that they do not cross at the source location. The main contributors are the cell size and the resolution in E_n.

Figure 5 shows the density of the elliptical lines, constructed with the superposition of 12 000 ellipses for the same simulated detector configuration. The contours represent various percentages of the maximum density. The image resolution is taken as the diameter of the 50% contour, divided by 2.35, and is ~12 cm. This value translates into an angular resolution of ~17 deg, a quantity that remains roughly invariant when imaging sources at a greater or shorter distance away

[a] Because the true energy spectrum is not strictly Maxwellian, it cannot be characterized by a single temperature. Jeki et al.[10] give a Maxwellian temperature of 1.57 MeV for energies >1 MeV and a temperature of 1.30 MeV otherwise. We use a spectrum that is an average of these two distributions.

[b] Reference 12 gives the value of 15 000 photon/MeV_{ee} in anthracene (Nuclear Enterprises specifies 65% of this as the value for NE-102). Birks's value[13] is perhaps too high by a factor of 2 or more. Our own measurements of light output in Bicron BC-408 (similar to NE-102) indicate that 9800/MeV_{ee} (= 65% of 15 000) may be too high by a factor of 2.

[c] The formula Bengston and Moszynski give and test was for paper-wrapped scintillators, not those wrapped in a reflective material such as aluminum foil. Pulses from foil-wrapped elements may have long tails from later-arriving photons. In such a case, the timing resolution may be a factor of 2 worse than that given by the formula.

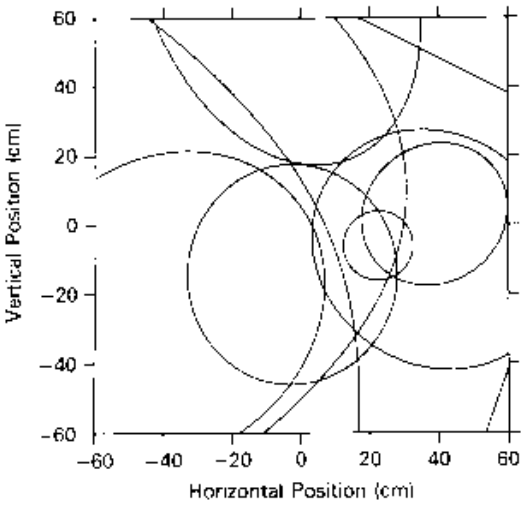

Fig. 4. Monte Carlo simulation of the ellipses that would result from a detector similar to the one shown in Fig. 1 when used with a point source located at a position (+15 cm, +15 cm) in the plane. Here the elements are made of NE-102 commercial scintillator, 4 cm thick, 4 cm high, and 5 cm long, which are arranged in a 10 × 10 grid in each detector plane. The planes are separated by a 12-cm gap, and the source is 40 cm from the front of the first plane. The ellipses no longer cross at the source location.

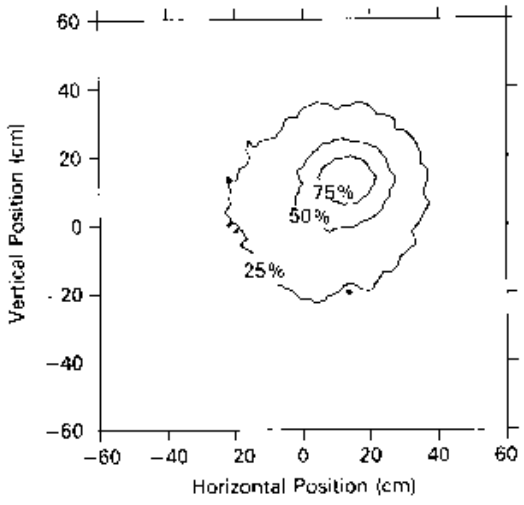

Fig. 5. The density plot constructed for the simulated detector configuration of Fig. 1. The figure here represents 12 500 ellipses constructed in the source plane by the detector. The source is located at (+15 cm, +15 cm).

from the detector. When imaging a distributed rather than a point source, the image size increases significantly if the source subtends an angle comparable to or greater than this value.

Three modifications to the configuration were tested. In the first, the gap between planes was doubled to 24 cm. In the next, the thickness of the cells was halved to 2 cm while the gap remained at 12 cm. In the last, all cells not on the corners were discarded, which left only the four corner cells per plane. Cell thicknesses were 4 cm and the gap was 12 cm.

The effects of the modifications are summarized in Table I. In this table, the efficiency is calculated with the source at the coordinates (+15 cm, +15 cm) in a plane 40 cm in front of the first detector plane and is stated on the basis of per neutron incident on the detector.[4] The "Rate" in the table is the detection rate per 10^5 n/s emitted from an isotropic source. The "Image Resolution" is derived from the diameter of the 50% contour divided by 2.35 as discussed earlier. In general, increases in pointing ability are at the expense of lesser efficiency. The last modification, which is designed to give simplicity in the electronics and hardware, gives quite a low efficiency and would only be useful for high source strengths combined with long counting times.

The pointing ability of the detector can be improved by raising the minimum pulse-height requirement for the front plane because the larger pulse heights will give better E_p resolution. For the case of the detector with the 24-cm gap between planes, the addition of a 350-keV$_{ee}$ cut on the pulse height in the front plane results in an image resolution of 9 deg. The detection efficiency, however, drops by 73% in comparison with the value in Table I.

It appears likely that an image resolution of better than 10 deg is within the capabilities of this type of detector. However, how good of a pointing ability is needed and how high of an efficiency is needed will be determined by the particular application.

V. EXPERIMENTAL

We have not yet constructed a detector of the complexity and expense described in the Sec. IV. Instead,

[4]The rate at which neutrons are detected when emitted from an isotropic source is taken as the product of this efficiency, the rate at which neutrons are emitted from the source, and the fraction of solid angle subtended by the front plane of the detector. For the baseline case and the first two modifications, this fraction is $\frac{1}{16\pi}$. The "detection rate" is the rate at which events trigger the detector and then pass sufficient software cuts to be identified as a neutron double scatter. The detection rate then depends on the stringency of the cuts. In this case, only the multiplicity cut and the 130-keV$_{ee}$ pulse-height cut were applied.

TABLE I

Detection Efficiencies and Angular Pointing Capabilities for the Baseline Detector and Three Modifications to It

Configuration	Efficiency[a] (%)	Rate[b] (Hz)	Image Resolution[c] (deg)
100 cell/plane 4-cm thickness 12-cm gap (baseline case)	1.58	96	17
100 cell/plane 4-cm thickness 24-cm gap (baseline case)	1.01	61	11
100 cell/plane 2-cm cell thickness 12-cm gap (baseline case)	0.80	48	15
4 corner cell/plane 4-cm thickness 12-cm gap (baseline case)	---	0.154	17

[a]Detection efficiency per neutron incident on the detector.

[b]Rate is the product of 10^5 n/s, the fraction of the solid angle subtended by the detector with the source at (+15 cm, +15 cm) in a plane 40 cm in front of the detector ($\sim \frac{1}{16.5}$ for the first three cases), and the efficiency.

[c]Image resolution taken as $\arctan(\sigma/40\ \text{cm})$, where σ is the diameter of the 50% contour divided by 2.35.

we rely on the use of an acceptable substitute detector to test the applicability of our simulation code and our assumptions about detector behavior. We use a neutron detector that is designed for another application (in the 100-MeV range) that has some major differences from the detector described earlier.

The detector is shown schematically in Fig. 6. It consists of two planes, containing four 4-cm-thick, 4-cm-high, 50-cm-long cells per plane. The scintillator material is Bicron BC408, which is similar to NE-102. The gap between the planes is 20 cm. Each cell has two PM tubes ($\frac{1}{4}$-in. Amperex XP2972-02), located at opposite ends of the cells. The anode signals pass into a splitter box and then into two custom-made amplifiers with gain factors of 200. The output from one amplifier leads to a constant-fraction discriminator, which then leads through ~150 ns of delay to a time-to-digital converter (TDC) stop. The other output leads through ~160 ns of delay into an analog-to-digital converter (ADC). Each cell therefore has two ADC channels and two TDC channels associated with it. The trigger requires both ends of a cell in the front plane

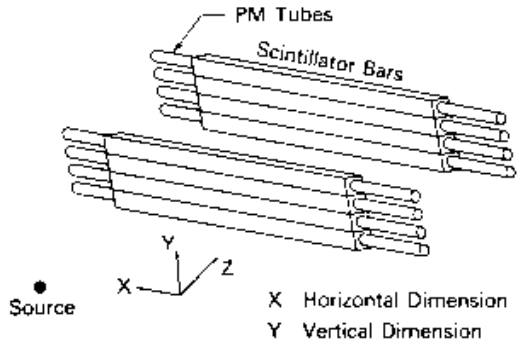

Fig. 6. Schematic drawing of the experimental detector. The time difference between the ends is used to find the hit position within a cell. The gap between the planes is 20 cm, and a ^{252}Cf source is located 20 cm from the front plane.

along with both ends of a cell in the second plane to fire discriminators. The TDCs are all started with the trigger and stopped by the individual end's discriminator output.

Hit positions within a cell are determined by the time difference between the two ends in a manner that is described in some detail elsewhere.[14] The hit position is given by the time difference multiplied by one-half the effective velocity of light in the scintillator (the "delta-t" method). The position resolution for our bars was measured as $\sigma_x = 15$ cm for a ^{137}Cs (662-keV gamma-ray) source.[6] The resolution is this poor because of low light collection efficiency in the bars due to the use of $\frac{1}{4}$-in. PM tubes that are much smaller than the bar cross section. From some ADC-based measurements, it was estimated that there are only 55 photoelectron/MeV$_{ee}$ in this detector. We found, however, that the detector still works satisfactorily in some geometries.

The light output of a pulse in a cell is taken as proportional to the geometric mean of the net ADC values in each end. The gain scale of each cell is set and monitored by collecting ^{137}Cs pulse-height spectra in singles mode and comparing the Compton edge location to the location of a Monte Carlo-calculated spectrum with the same energy resolution. It is determined from the Monte Carlo studies that the gain scale should be set so that the three-quarters height of the Compton edge corresponds to 478 keV$_{ee}$, which is in agreement with the findings in Ref. 3.

The measurements to date were made using a

[6]This energy was chosen because the resulting light outputs are comparable to those for the average recoil proton.

^{252}Cf source with a strength of 630 ± 60 fission/s. Because of the concern with false coincidence events involving gamma rays emitted in the fission process, measurements were made with a shielded source as well as with the bare source. The shield was a square slab of lead, ~5 cm on a side and 8 mm thick in the direction of neutron travel. This thickness was chosen to eliminate 80% of the gamma rays while scattering or absorbing <5% of the neutrons. Because the lead preferentially absorbs the lower energy gamma rays, the energy spectrum of the surviving gamma rays is harder than that from the unshielded source. These gamma rays tend to produce a large pulse height compared to a recoil proton. Experimental measurements were made with and without the lead shield of the ^{252}Cf singles pulse-height spectrum in one of the cells in the detector array. When the measurements were compared to Monte Carlo predictions, it was confirmed that the lead shield was working as expected.

Before restrictive timing was included in the coincidence gate, the hardware trigger rate from room background was ~50 Hz, mostly due to environmental gamma rays and cosmic rays. The computer dead time was >30% under these circumstances. To reduce the rate, the coincidence gate was modified to require a minimum delay of ~4 ns after the firing of a cell in the first plane before the firing of a cell in the second plane. This modification reduced the background trigger rate to ~0.8 Hz. The trigger rate with the unshielded source placed 20 cm away from the center of the front plane of the detector was 3.1 Hz, and the livetime was 100%. When the lead shield was used, the trigger rate was 2.0 Hz.

The disposition of events is summarized in Table II. The "net" rates are the "gross" rates minus the background rates. The table also shows the effects of restrictions applied by the sorting software.

The two main software cuts are (a) that the number of cells triggered per plane must be unity (test 1) and (b) that the calculated incident neutron energy ($E_i = E_p + E_n$) is <10 MeV (test 2). Gamma- and cosmic-ray events are virtually eliminated because their short TOF translates into a very large equivalent E_n. For the shielded source, the multiplicity requirement eliminates about one-sixth of the net triggers, and the energy requirement eliminates ~6% of the remaining events. These cuts eliminate a greater fraction of the net triggers when the bare source is used.

Figure 7 shows the recoil-proton energy spectrum in the front plane of the detector for the shielded (live time of 23.8 h) and unshielded source (live time of 18.2 h) for those events that pass the above software tests, normalized to 23.8-h live time. The lead shield

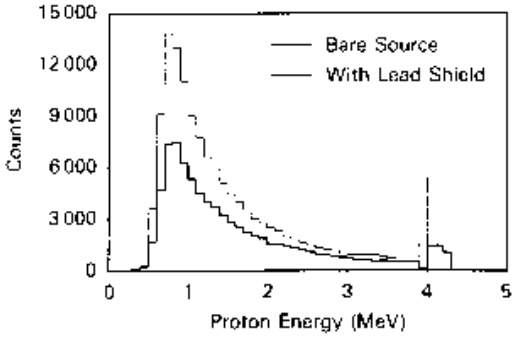

Fig. 7. Recoil-proton energy spectrum obtained in the front plane of experimental detector for those events that are determined to be valid neutron double scatters. The proton energy is calculated from the pulse intensity, which is then inverted using a proton light output curve. The effect of the lead is to greatly reduce the gamma-ray flux and thereby the number of gamma-ray/neutron coincidences that pass as neutron double scatters.

TABLE II

Trigger Rates and Event Rates Passing the Main Software Tests for a ^{252}Cf Source 20 cm in Front of the Experimental Prototype Detector With and Without 8-mm Lead Shielding

Measurement Type	Bare Source		With 8-mm Lead Shield		Background, Gross
	Gross	Net	Gross	Net	
Trigger rate (Hz)	3.05	2.24	2.00	1.19	0.81
Test 1: unit multiplicity in each plane	2.38	1.78	1.61	1.00	0.60
Test 2: test 1 and incident energy <10 MeV	1.66	1.54	1.06	0.94	0.121
Test 3: test 2 and proton energies such that $0.8 < E_p < 3.7$ MeV and $0.8 < E_{p,2}$	0.84	0.80	0.56	0.52	0.038
Test 4: test 3 and back plane proton energy such that $E_{p,2} < 2E_n$	0.50	0.48	0.39	0.37	0.019

eliminates a higher percentage of events with lower effective proton energies (lower pulse heights). The events with higher than 3.9-MeV proton energy (1.40 MeV_{ee}) have fallen into the overflow channel of one or both ADCs. From Monte Carlo studies of the detector, it is determined that the true neutron double scatters are very unlikely to give 1.4-MeV_{ee} pulse height in either plane, and therefore the events in the overflows are probably due to other coincidences.

Test 3 in Table II is designed to eliminate the hardware effects caused by discriminator thresholds and ADC overflows. An 0.8-MeV minimum proton energy (corresponding to the 0.13-MeV_{ee} pulse-height range) in *both* planes is used to insure that the calculation and experiment are on the same basis regarding the discriminator thresholds. Only with this cut can a comparison between the measured and calculated efficiencies be made. The proton energy in the *front* plane is also required to be <3.7 MeV (1.30-MeV_{ee} pulse height).

Figure 8 shows the proton energy spectrum again with this additional software cut added. The Monte Carlo calculated spectrum shown in Fig. 8 is normalized to the same number of neutrons emitted from the source as in the experiment. All three software tests included for the experimental data are included for the Monte Carlo calculation. The calculated detection rate is 0.079% per fission event, which emits on the average 3.85 neutrons. The uncertainty on the calculation can be taken as 15%, with 10% due to the uncertainty in the source strength and 10% due to the uncertainty in the energy spectrum.[10]

Only 5% of the simulated events (compared with >16% of the net experimental triggers) fails the multiplicity test. This 5% failure rate must represent single neutrons that scatter in at least three cells because in the Monte Carlo code only one neutron is emitted from the source at a time. The 11% excess of events failing this test experimentally must be caused by separate particles that are emitted in the same fission event.

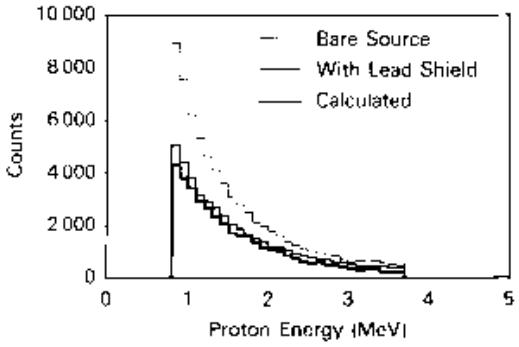

Fig. 8. The same spectrum as in Fig. 7 except that a proton energy cut of 0.8 MeV $< E_p <$ 3.8 MeV on both planes was used. Also shown is the Monte Carlo–calculated spectrum for the same number of source fission events. The proton energy cut is used to render a valid comparison between the experimental and calculated curves. There is an excess number of counts in the experimental spectra probably due to coincidences between different particles.

The experimental spectra have greater numbers of counts than the Monte Carlo calculation predicts, presumably because of false coincidences between gamma rays and neutrons or two neutrons emitted during the same fission event. An estimate of the relative importance of these false coincidences can be made by comparing the foregoing calculated neutron double scatter rate (per fission) with the product of the singles rates (per fission) in the two planes. If these numbers are comparable, the likelihood of significant contamination from the false coincidence events is indicated. The calculated neutron singles rates in the first and second planes are 8 and ~1% per fission, respectively. The product of these two rates is ~0.08% per fission, a number roughly equal to the detection rate obtained with the Monte Carlo code result as shown in Fig. 8. The product of the calculated gamma-ray singles rate in the front plane (not including the effect of the lead shielding) with the neutron singles rate in the back plane is ~0.17% per fission. The lead shielding reduces this product to 0.05% per fission.

To check experimentally for the presence of false coincidences, the detection rate was measured with the unshielded source moved back to 60 cm from the front plane of the detector. Primarily because of solid angle factors, the absolute efficiency for detection of coincidences between two different particles should drop by a factor of ~20, while the desired neutron double scatter efficiency should drop by a factor of ~5. The measured rate at this source location with the aforementioned software cuts was ~10% below the Monte Carlo–calculated rate. When the source was in the closer position, the rate had been 80% higher than the calculation. It is therefore concluded that the first three software cuts are insufficient to eliminate false coincidences.

A method to eliminate many undesired coincidences was found by examining the experimental data for both source locations in comparison with the Monte Carlo predictions. The spectrum of the variable $x_2 = (E_{p,2}/E_n)^{1/2}$ is shown in Fig. 9 for the same data set that was presented in Fig. 8. This variable is the square root of the scattered proton energy in the back plane divided by the energy of the neutron that is supposed to be causing the scatter. Theoretically, this quantity should never exceed unity, but when resolution effects are included, it can be as great as 1.4. The experimental tail on this distribution must represent coincidences that are not neutron double scatters.

To reduce the number of undesired coincidences from the experimental spectrum, another test (test 4

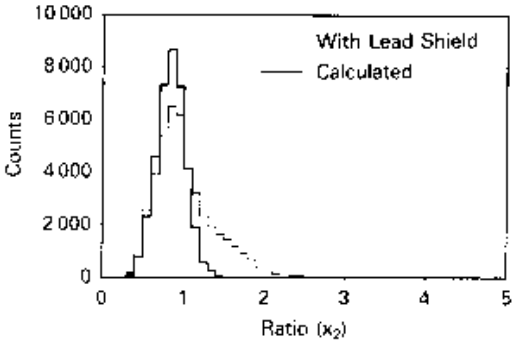

Fig. 9. Spectrum for the quantity $x_2 = (E_{n,1}/E_n)^{1/2}$ with the same software cuts. The excess counts in the experimental spectrum often have x_2 values greater than expected for true neutron double scatters. The addition of a software cut on x_2 is suggested by this plot.

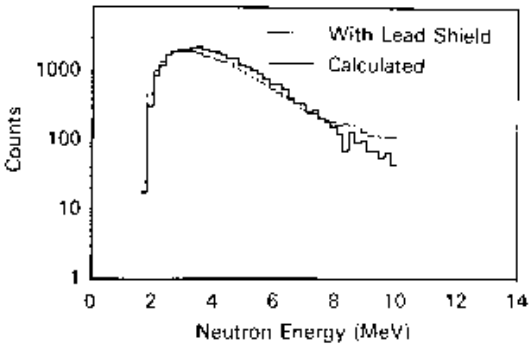

Fig. 10. Reconstructed incident neutron energy spectrum for the shielded ^{252}Cf source with the final software cuts. The incident energy is taken as the proton energy in the front plane calculated from the pulse height plus the scattered neutron energy determined from the TOF. Calculated and measured spectra are seen to have close to the same efficiency, but the uncertainty in the calculation is ±15%.

in Table II) was introduced that includes the restriction that $x_2 < 1.4$. Other minor cuts of this nature were also included. This final set of cuts eliminated ~30% of the events in the experimental spectrum from the shielded source (~50% for the unshielded source) that remained from the previous cuts. Only 8% of the corresponding Monte Carlo events were eliminated.

The reconstructed incident neutron energy spectrum with these software requirements is shown for the shielded source in Fig. 10. The calculated detection rate is 0.066% per fission event.[1] The measurement gives ~0.059% with the lead shield (0.077% without). The disagreement between the calculated and the measured rates can be explained almost exactly by the 11% difference in the probability of passing the multiplicity test.

The effective 2-MeV threshold energy for this detector with these software cuts makes the calculated rate somewhat sensitive to the Maxwellian temperature, so that using a temperature of 1.57 MeV in the calculations would increase the rate by 10%. The measured compared with calculated rates would still essentially agree to within the ±10% source strength uncertainty. The shape of the spectrum would agree more precisely at higher energies by assuming the higher temperature.

The solid contours in Fig. 11 show the density of the elliptical lines constructed in the source plane for events passing all the software cuts discussed earlier. In this measurement, the source was located at 19 cm to the right of center in the image plane, which is 20 cm in front of the detector. The contours are at 25, 50, and 75% of the maximum density. The point of maximum density in this plot is very near the true source position. The large image size is primarily due to the poor hit position resolution within the cells.

The dotted contours show the results of the Monte Carlo simulation as applied to the stated experimental configuration. The shapes of the distributions and the location of the maxima are in good agreement between the experiment and simulation. The differences (and some of the differences in Fig. 10) can be due to using the inverse of a proton light output curve taken from the literature to determine the proton energies from the pulse heights in the experiment. We have not made measurements to verify this curve. The corresponding process when using the Monte Carlo code is essentially exact (neglecting resolution effects).

Even with its poor hit position resolution, the detector is capable of counting whether there are one or two sources present if the sources are separated by at least 19 cm. This capability is illustrated in Fig. 12. Shown is a projection onto the x (horizontal) axis of the experimental data shown in Fig. 11 with its maximum located at 19 cm. Also shown is the same distribution (for a different experimental run) with the source located at $x = 0$. The third curve is the sum of the first two curves, taken to represent the image from two sources. The summed distribution is broader than either single-source distribution. By analysis of the

[1]The detection rate per emitted neutron is then 0.017% because there is an average of 3.85 n/fission. For the purposes of comparing this detector with those in Table I, the "efficiency" can be stated as 0.19% per neutron incident on the detector.

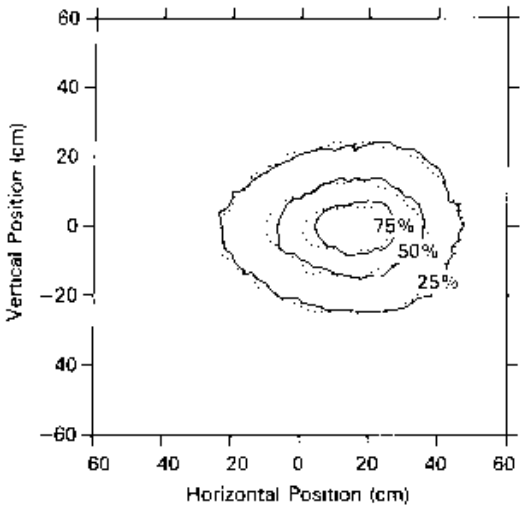

Fig. 11. Density plot of data obtained in experimental setup (solid lines) with the source located at (+19 cm, 0 cm) at a 20-cm distance from the front plane. The Monte Carlo simulation (dotted lines) as applied to the above experimental configuration is also shown. The contours shown represent percentages of maximum density. The shapes of the distributions and the location of the maxima tend to confirm the accuracy of the simulation code.

width and shape, one could determine that there is greater than one source present, provided that there is confidence in the detector response.

VI. DISCUSSION AND CONCLUSIONS

The Monte Carlo code has given us a tool to use to compare various designs. The experimental measurements have demonstrated the feasibility of a neutron imaging detector concept and have tested computer algorithms that could be used with an operating detector. The measurements confirm a reasonable degree of accuracy of the Monte Carlo code in its prediction of pulse-height distributions, neutron detection efficiency, and image resolution.

Between the experimental and modeling work, we reached some general conclusions about detector design. The trigger rate from room-background events can be substantially reduced by a suitable time-delayed coincidence. Further background reductions can be achieved by software TOF and pulse-height tests. The use of the delta-t method for finding hit positions significantly diminishes the image quality for fission spectrum neutrons and is not recommended. The false coincidences between a gamma ray and a neutron or between two neutrons emitted in the same fission can distort image quality. The gamma flux, especially at lower energies, can be reduced by using lead shielding without significantly absorbing or scattering the neutron flux. The use of a scintillator material that allows pulse-shape discrimination to eliminate gamma-ray events can be recommended.

When an actual detector is designed, trade-offs must be made between detection efficiency and angular image resolution. In general, improving one diminishes the other unless the complexity of the detector increases. For instance, using smaller cells gives improved angular resolution and decreases efficiency unless more cells are added to the array. A larger gap between planes has the same effect. The addition of software requirements, such as raising the effective discriminator threshold, can produce enhanced image quality but always at the expense of efficiency. Depending on the specific application, it may or may not be useful to add in such requirements.

The image in Fig. 5 (from the simulation) was obtained with 12 000 ellipses superimposed. The efficiency results in Table I show that if the neutron source strength for a nuclear warhead is $\sim 10^5$ n/s, the image can be collected in ~2 min. Hopefully, this speed is adequate, and higher efficiency is not needed. The total singles rate in the front plane should be ~1500 Hz, and in the back plane ~700 Hz, under the assumption that

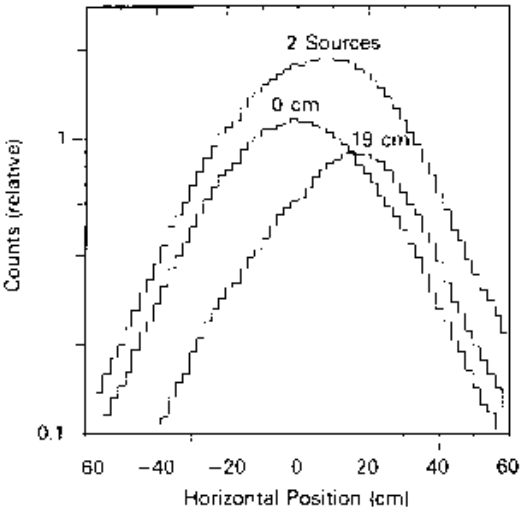

Fig. 12. Projection onto the x axis of the experimental density plots obtained with source positions (+19, 0 cm) and (0, 0 cm). Also shown is the summation of the two individual spectra, taken to represent the expected spectra for two sources measured simultaneously. A careful analysis of the width and shape of the spectra could distinguish whether there are one or two sources present.

the singles detection efficiency is ~25% (for either neutrons or gamma rays) per plane. A resolving time of 50 ns gives an accidentals rate of <1 Hz; designs with higher efficiencies than shown in Table I will therefore give faster results without excessive problems from accidental coincidences.

In practice, the neutron and gamma-ray source strength can be substantially higher than these estimates, depending on weapon design and age. There also can be strong gamma-ray and neutron backgrounds present, which are produced by nuclear weapons or materials that are stored nearby. These circumstances can lead to accidental rate or computer dead-time problems. Only by field testing can these issues be addressed.

There are some unresolved neutron transport problems. The neutron sources within a warhead are distributed rather than point sources. The effects of neutron scattering within the warheads or missile can be significant and energy dependent. Reflected neutron fluxes will be present if the measurements are to be made in a confined area.

Practical considerations in the detector design include minimizing the mass of the structure and the PM tubes in relation to the scintillator mass. The detector, electronics, and analyzer must be integrated into a portable unit for field use.

The real design problem is more complicated than simply optimizing performance. The quality of image that the detector is allowed to produce can be limited if there is concern about revealing sensitive information about warhead or missile design. The incident neutron flux will be determined by how closely the detector is to be placed near the missile. This, in turn, can be determined by practical or by political constraints.

ACKNOWLEDGMENTS

We thank D. Drake for providing us with the original idea and J. Simmons for his interest and useful contributions; P. Dyer's help with the source strength determination is greatly appreciated.

This work was partially supported by the Office of Arms Control of the U.S. Department of Energy under B&R Code GC010110 and by the Defense Advanced Research Projects Agency under Work Order 5302.

REFERENCES

1. R. T. GRANNAN, R. KOGA, W. A. MILLARD, A. M. PRESZLER, G. M. SIMNETT, and R. S. WHITE, *Nucl. Instrum. Methods*, **103**, 99 (1972).

2. A. M. PRESZLER, S. MOON, and R. S. WHITE, *J. Geophys. Res.*, **81**, 4715 (1976).

3. G. DIETZE and H. KLEIN, *Nucl. Instrum. Methods*, **193**, 549 (1982).

4. J. TERRELL, *Phys. Rev.*, **108**, 783 (1957).

5. K. SKARSVAG, *Phys. Rev. C*, **22**, 638 (1980).

6. H. MAIER-LEIBNITZ, P. ARMBRUSTER, and H. J. SPECHT, "Prompt and Delayed Gamma-Rays from Fission," *Proc. Symp. Physics and Chemistry of Fission*, Salzburg, Austria, March 22-26, 1965, Vol. 2, p. 113, International Atomic Energy Agency (1965).

7. W. C. SAILOR, R. C. BYRD, and Y. YARIV, "Calculations of the Pulse-Height Response of Organic Scintillators for Neutron Energies $28 < E_n < 492$ MeV," LA-UR-88-3719, Los Alamos National Laboratory (1989).

8. R. A. CECIL, B. D. ANDERSON, and R. MADEY, *Nucl. Instrum. Methods*, **161**, 439 (1979).

9. R. MADEY, F. M. WATERMAN, A. R. BALDWIN, J. N. KNUDSON, J. D. CARLSON, and J. RAPAPORT, *Nucl. Instrum. Methods*, **151**, 445 (1978).

10. L. JEKI, Gy. KLUGE, A. LAJTAI, P. P. DYACHENKO, and B. D. KUZMINOV, "Fission Neutron Spectrum Measurement of ^{252}Cf," *Proc. Mtg. Prompt Fission Neutron Spectra*, Vienna, Austria, August 25-27, 1971, International Atomic Energy Agency (1972).

11. G. F. KNOLL, *Radiation Detection and Measurement*, John Wiley and Sons, New York (1979).

12. J. B. BIRKS, *The Theory and Practice of Scintillation Counting*, Pergamon Press, London (1964).

13. B. BENGSTON and M. MOSZYNSKI, *Nucl. Instrum. Methods*, **81**, 109 (1970).

14. T. N. TADDEUCCI et al., *Nucl. Instrum. Methods*, **A241**, 448 (1985).